Combustion and Flame 259 (2024) 113168

Contents lists available at ScienceDirect

Combustion and Flame

journal homepage: www.sciencedirect.com/journal/combustion-and-flame

Foundational Fuel Chemistry Model 2 – *iso*-Butene chemistry and application in modeling alcohol-to-jet fuel combustion

Yue Zhang [a], Wendi Dong [a], Rui Xu [a,1], Gregory P. Smith [b], Hai Wang [a,*]

[a] Department of Mechanical Engineering, Stanford University, Stanford, CA 94305, United States of America
[b] SRI International, Menlo Park, CA 94025, United States of America

ARTICLE INFO

Keywords:
Foundational fuel chemistry model
Alcohol-to-jet fuel
Uncertainty minimization
Optimization
Chemical kinetics

ABSTRACT

The Hybrid Chemistry (HyChem) approach is applied to model the combustion chemistry of Gevo's alcohol-to-jet (ATJ) fuel, a conventional Jet A fuel, and their blends. The focus of the current study is on the foundational fuel chemistry submodel in the HyChem approach. Specifically, the newly developed Foundational Fuel Chemistry Model 2 (FFCM-2) is used as the base model for describing the high-temperature pyrolysis and oxidation kinetics of hydrogen, carbon monoxide, formaldehyde, and C_{1-4} hydrocarbons. Key issues addressed and resolved include difficulties of a previous kinetic model in accurately predicting the pyrolysis kinetics and combustion properties of *iso*-butene, which is the key intermediate in the combustion of the ATJ fuel. Additionally, we show that FFCM-2, being fully assessed for its kinetic uncertainty, enables us to quantify the uncertainties of the HyChem models of both real fuels.

1. Introduction

In an earlier work we proposed a physics-based Hybrid Chemistry (HyChem) approach to modeling real liquid fuels [1,2]. The approach leverages the fact that high-temperature combustion of large hydrocarbons and real liquid fuels proceeds in two separate stages: the fuel first decomposes into intermediate fragment species which are consisted of primarily H_2, C_{1-4} hydrocarbons, benzene and toluene (referred to as foundational fuels), followed by the oxidation of the fragments. These two steps can be modeled separately: the fast fuel decomposition may be described by several global, lumped reactions based on speciation measurements. The oxidation of the fragments is rate-limiting and thus must be treated with a detailed chemistry model. To illustrate the above point, Fig. 1 shows the species time-history during oxidation of Gevo's alcohol-to-jet (ATJ) fuel and a conventional aviation fuel Jet A, where the experimental data are taken from previous studies [2,3] and the simulation results are from HyChem model predictions [2,3]. Clearly, fuel decomposition is temporally separable from the oxidation of the pyrolysis products. HyChem removes the difficulty in defining the composition of real fuels; it relies on the more direct speciation data that define the combustion chemistry properties of a real fuel. The HyChem approach significantly reduces the number of species and reactions which are often difficult to study from first-principles or experiments; and it has been successfully applied to model a series of real fuels, from conventional jet fuels [1,2], synthetic jet fuels [4], rocket fuels [2], gasoline fuels [5], and sustainable aviation fuels [3], to NO_x formation from Jet A combustion [6]. HyChem models have also been used in some of the recent direct numerical simulations of turbulent combustion problems and computational fluid dynamics of real-fuel combustion behaviors in complex combustors (see, e.g., [7–16]).

Earlier HyChem studies used USC Mech II [17] as the foundational fuel chemistry model. While the resulting HyChem models were able to predict a range of combustion property data, including laminar flame speed, non-premixed flame extinction strain rates, and ignition delay time, a key issue identified was that the model prediction uncertainties remain large. These uncertainties stem largely from the rate parameter uncertainties in USC Mech II [2,3,18]. Another issue is the deficiency of USC Mech II in the *iso*-butene (i-C_4H_8) chemistry. Gevo ATJ consists primarily of two highly-branched alkanes: *iso*-dodecane (i-$C_{12}H_{26}$) and *iso*-cetane (i-$C_{16}H_{34}$) [3,19]; its high-temperature decomposition yields i-C_4H_8 as a major intermediate species (see, Fig. 1).

The aforementioned issues with USC Mech II led us to re-examine the foundational fuel chemistry model in recent years. FFCM-1 [20,21] was such an effort, but the fuel coverage of the FFCM-1 model is narrow and ranges from H_2, syngas, to CH_4 only. Very recently, we developed Foundational Fuel Chemistry Model version 2.0 (FFCM-2) [22]. FFCM-2 assembles the state of kinetic knowledge in C_{0-4} fuel combustion

* Corresponding author.
E-mail address: haiwang@stanford.edu (H. Wang).
[1] Current address: Department of Chemistry and the PULSE Institute, Stanford University, Stanford, CA 94305, USA; SLAC National Accelerator Laboratory, Menlo Park, CA 94025, USA.

https://doi.org/10.1016/j.combustflame.2023.113168
Received 26 July 2023; Received in revised form 23 October 2023; Accepted 24 October 2023

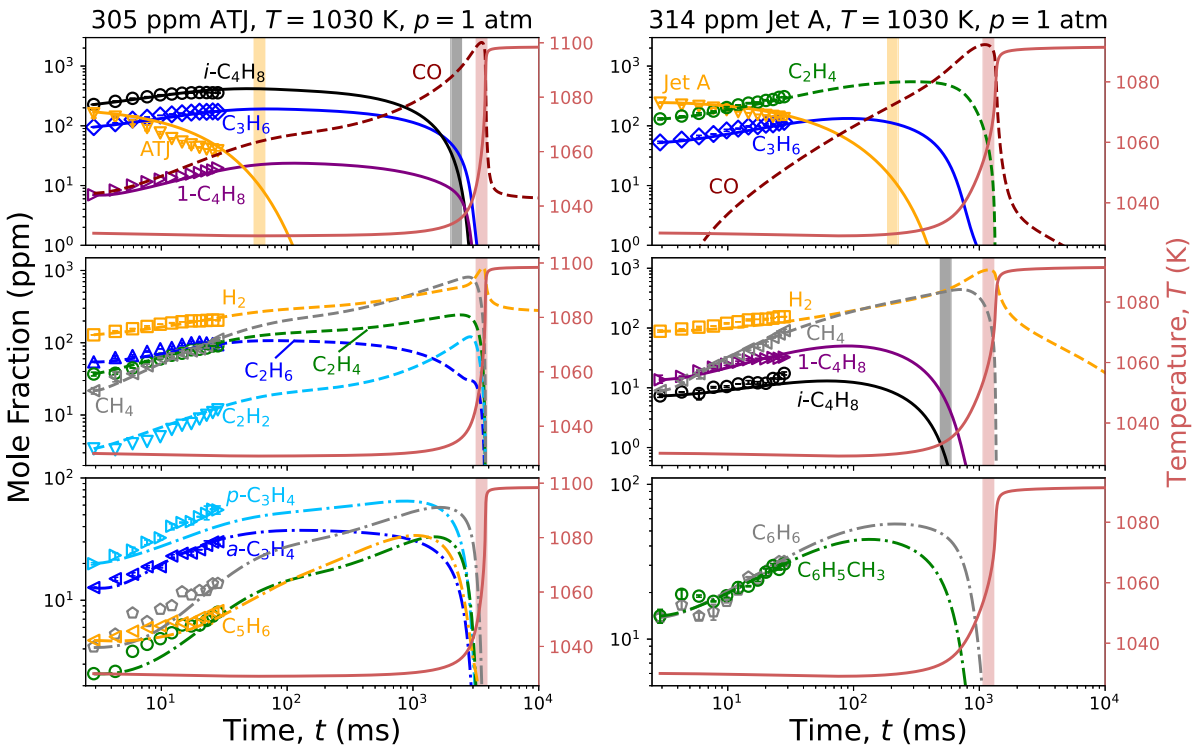

Fig. 1. Flow reactor species time–history predicted by the earlier, USC Mech II based HyChem ATJ and Jet A models for the oxidative pyrolysis of 305 ppm ATJ (left column) and 314 ppm Jet A (right column) in a vitiated oxygen–nitrogen mixture at temperature T = 1030 K and pressure p = 1 atm. The symbols and lines are experimental data and model predictions for Jet A from [2] and ATJ from [3], respectively. Error bars indicate 2σ uncertainty of the data, many of which are smaller than the symbol sizes.

chemistry into a reaction model, and improves its prediction accuracy by assimilating a wide range of legacy combustion property data into the model through a rigorous parameter optimization and uncertainty minimization study. Optimization and uncertainty minimization used a version of the Method of Uncertainty Minimization using Polynomial Chaos Expansions (MUM-PCE) [23,24] that is now extended to the use of neural network (NN)-based response surfaces [25]. The NN-MUM-PCE improved the overall accuracy, efficiency, and scalability of the original MUM-PCE and enabled the optimization of FFCM-2 against 1192 fundamental combustion property targets over a wide range of thermodynamic conditions.

A key objective of the current work is to examine closely the i-C_4H_8 chemistry in FFCM-2, and in doing so, re-examine the HyChem model for the ATJ fuel. In the current work, we advanced a systematic approach to deriving the HyChem model parameters through the solution of an inverse problem using an improved foundational fuel chemistry model. A conventional aviation fuel Jet A is included in the current analysis because of the interest in ATJ-Jet A fuel blends. Lastly, we assess the impact of reduced prediction uncertainty of the optimized FFCM-2 on the prediction uncertainty of the updated HyChem models.

2. Methods

2.1. iso-Butene chemistry

In this section, we briefly summarize the FFCM-2 effort, and illustrate the development process using the i-C_4H_8 sub-model as an example. The optimized FFCM-2 and additional details, including the full list of the optimization targets, are available at https://web.stanford.edu/group/haiwanglab/FFCM2/ [22]. Separately, the HyChem parameters were determined subsequently for two aviation fuels using methods to be discussed later in this section.

The trial FFCM-2 comprises of 96 species and 1054 reactions, covering the combustion chemistry of relevant $C_{0\text{-}4}$ foundational fuels [22]. The trial model was compiled after reviewing the state of knowledge for the foundational fuel reaction kinetics. The reactions and their rate constants were sourced from 227 publications that date back to 1960 [22]. Legacy fundamental combustion property data (laminar flame speed, shock tube ignition delay time and species time–history measurements) were collected, resulting in the Stanford Fundamental Combustion Property Database (SFCPD) that consists of 2148 sets of data dating back to 1937 [22]. A total of 1192 optimization targets were selected from this database, and the coverage of the optimization targets is provided in Table S1 of the Supplementary Materials (SM). For each selected target, experimental uncertainty was evaluated, taking into consideration the statistical consistency among the data and the underlying measurement techniques. More details about optimization targets and additional test data are available from the FFCM-2 website [22].

For the current work, we focus on the reaction kinetics of the i-C_4H_8 submodel of FFCM-2. Relevant combustion property data [26–37] are discussed in Section S2 of the Supplementary Materials (SM). Highlighted below are several key reaction for i-C_4H_8 pyrolysis and oxidation, and the source of the trial model rate parameter assignments. In a recent work, Nagaraja et al. [30] measured the products formed during the pyrolysis of 2% i-C_4H_8-98% Ar at pressure p_5 = 2 atm, temperature T_5 = 982 – 1764 K, and residence time around 3 ms, in a single-pulse shock tube. They found that the isomerization of i-C_4H_8

$$i\text{-}C_4H_8 \rightleftharpoons 1\text{-}C_4H_8\ , \tag{1}$$

$$i\text{-}C_4H_8 \rightleftharpoons 2\text{-}C_4H_8\ , \tag{2}$$

$$1\text{-}C_4H_8 \rightleftharpoons 2\text{-}C_4H_8\ , \tag{3}$$

could be critical to the destruction of i-C_4H_8. In FFCM-2, the rate constants of these reactions were determined by combining reaction rate theory analysis with constrained optimization against shock tube speciation data. The trial rate constants were calculated through a

Table 1
HyChem parameters and their physical limits.

Fuel	Descriptions	Parameters	Range[a]
ATJ	*A*-factors of the lumped ATJ reactions	$A_1 - A_7$	$[A_{k,0}/10,\ A_{k,0} \times 10]$
	Number of H produced in the C–C fission reaction per C_mH_n in reaction (14)	α_1	[0, 2]
	Number of H produced in the H-abstraction reactions per C_mH_n in reaction (15)	β_1	[0, 1]
	Ratio of C_2H_4 to i-C_4H_8	ω_2	[0, 1]
	Ratio of C_3H_6 to i-C_4H_8	ω_3	[0, 1]
Jet A	*A*-factors of the lumped Jet A reactions	$A_8 - A_{14}$	$[A_{k,0}/10,\ A_{k,0} \times 10]$
	Number of H produced in the C–C fission reaction per C_mH_n in reaction (16)	α_2	[0, 2]
	Number of H produced in the H-abstraction reactions per C_mH_n in reaction (17)	β_2	[0, 1]
	CH_4 yield per C_mH_n in addition to H abstraction by CH_3 in reaction (17)	γ	$[0,\ \gamma_{\max}]$[b]
	Ratio of C_3H_6 to C_2H_4	λ_3	[0, 1]
	Ratio of i-C_4H_8 to C_2H_4	$\lambda_{4,i}$	[0, 1]
	Ratio of 1-C_4H_8 to C_2H_4	$\lambda_{4,1}$	[0, 1]
	Ratio of C_6H_6 to C_6H_6 + $C_6H_5CH_3$	χ	[0, 1]

[a] For the stoichiometric parameters, the range values correspond to their physical bounds; while for the *A*-factors, the ranges correspond to allowed bounds (i.e. upper/lower by factor of 10) during HyChem parameter determination.
[b] $\gamma_{\max} = [-(4-\chi)m + (7-\chi)n/2 + 3\beta_2]/(10-\chi) - 1$ by setting $e_{a,2} \geq 0$ in reaction (17).

methylcyclopropane (MCP) intermediate on the basis of experimental observations [38] for MCP shock tube isomerization to the butene isomers. Quantum chemistry calculations on cyclopropane ring opening to propene [39] provided guidance for transition state parameters to the concerted hydrogen shift–ring opening process. We conducted master equation [40] calculations ($T = 1000 - 2000$ K, $p = 1 - 10$ atm) with the MultiWell code [41] to produce the initial rate parameters, thought to be peripheral at the time, adjusting the transition state parameters and barriers to mimic the MCP experimental results. Note for brevity our model uses a thermal average of the *cis*- and *trans*-2-butene and omits cyclic isomers.

The allylic-site hydrogen abstraction by H radical and the chemically activated addition reaction of H radical to i-C_4H_8

$$i\text{-}C_4H_8 + H \rightleftharpoons i\text{-}C_4H_7 + H_2, \tag{4}$$

$$i\text{-}C_4H_8 + H \rightleftharpoons C_3H_6 + CH_3 \tag{5}$$

were adopted from the RRKM [42–44] and master equation calculations by Power et al. [45]. The hydrogen abstraction reaction by CH_3

$$i\text{-}C_4H_8 + CH_3 \rightleftharpoons i\text{-}C_4H_7 + CH_4 \tag{6}$$

was from the rate constant calculations by Wang and Dean [46] based on CBS-QB3 level of theory [47].

Key reactions of i-C_4H_8 oxidation were carefully evaluated, taking into consideration multiple literature studies. For example, ignition delay times of i-C_4H_8/air mixtures are sensitive to the allylic-site hydrogen abstraction

$$i\text{-}C_4H_8 + O_2 \rightleftharpoons i\text{-}C_4H_7 + HO_2 \tag{7}$$

under elevated pressures and high oxygen concentrations [28,35]. The rate expression of Lokachari et al. [37] was adopted. The rate expression of hydrogen abstraction by OH,

$$i\text{-}C_4H_8 + OH \rightleftharpoons i\text{-}C_4H_7 + H_2O \tag{8}$$

was derived from a joint consideration of the shock tube measurements by Khaled et al. [48] and Vasu et al. [49]. Other rate assignments are discussed in [22].

2.2. FFCM-2 optimization and uncertainty minimization

The neural network based MUM-PCE (NN-MUM-PCE) [25] approach was used for optimization and uncertainty minimization of FFCM-2. Details are given in [22]. Briefly, $K = 1052$ rate parameters (1029 *A*-factors and 23 third-body Chaperon efficiencies) in the model were optimized against $M = 1192$ combustion property targets by solving a globally constrained minimization problem given as,

$$\min_{\mathbf{x}} \Phi_1(\mathbf{x}) = \min_{\mathbf{x}} \left\{ \sum_{m=1}^{M} \left(\frac{y_m(\mathbf{x}) - y_{m,obs}}{\sigma_{m,obs}} \right)^2 + \|\lambda \mathbf{x}\|_2^2 \right\}, s.t., \mathbf{x} \in [-\mathbf{1}, \mathbf{1}] , \tag{9}$$

where M is the number of experimental targets, $\mathbf{x} \in \mathbb{R}^K$ is the vector of normalized rate parameters, K is the number of rate parameters considered in optimization, including the *A*-factors of all reactions and selected third-body Chaperon efficiencies (β_M). We define the normalized rate parameters x_k and x_l as

$$x_k = \frac{\log(A_k/A_{k,0})}{\log f_k}, \tag{10}$$

$$x_l = \frac{\log(\beta_{M,k}/\beta_{M,k,0})}{\log f_{M,k}}, \tag{11}$$

where f_k and $f_{M,k}$ are the respective uncertainty factors, and $A_{k,0}$ are $\beta_{M,k,0}$ are the trial model assignments. The first term of Eq. (9) measures the residual sum of squares between the computed $y_m(\mathbf{x})$ and experimental target $y_{m,obs}$, inversely weighted by the squares of the standard deviation of the target $\sigma_{m,obs}$. The second term is introduced to prevent the optimization from over-fitting the targets, where λ is a regularization factor that provides weighting between the rate parameters and combustion property targets. In FFCM-2 optimization, $\lambda = 4$ was found to be an appropriate choice [22], as it provides roughly equal weighting between the first and second terms of Eq. (9). The computed $y_m(\mathbf{x})$ is represented by a response surface (or a surrogate model) using a fully-connected neural network, which maps $K = 1052$ active rate parameters to the computed combustion property using training samples generated from suitable Monte Carlo simulations [25].

To minimize model uncertainties, we assumed a multivariate log-normal distribution on $\mathbf{x}$ in the prior distribution. We could linearize the response surfaces after optimization, and express the optimized rate parameter as $\mathbf{x}^* = \mathbf{x}^{(\mathbf{0})*} + \mathbf{x}^{(\mathbf{1})*}\xi$, where $\xi \sim \mathcal{N}(0,1)$ is a standard normal

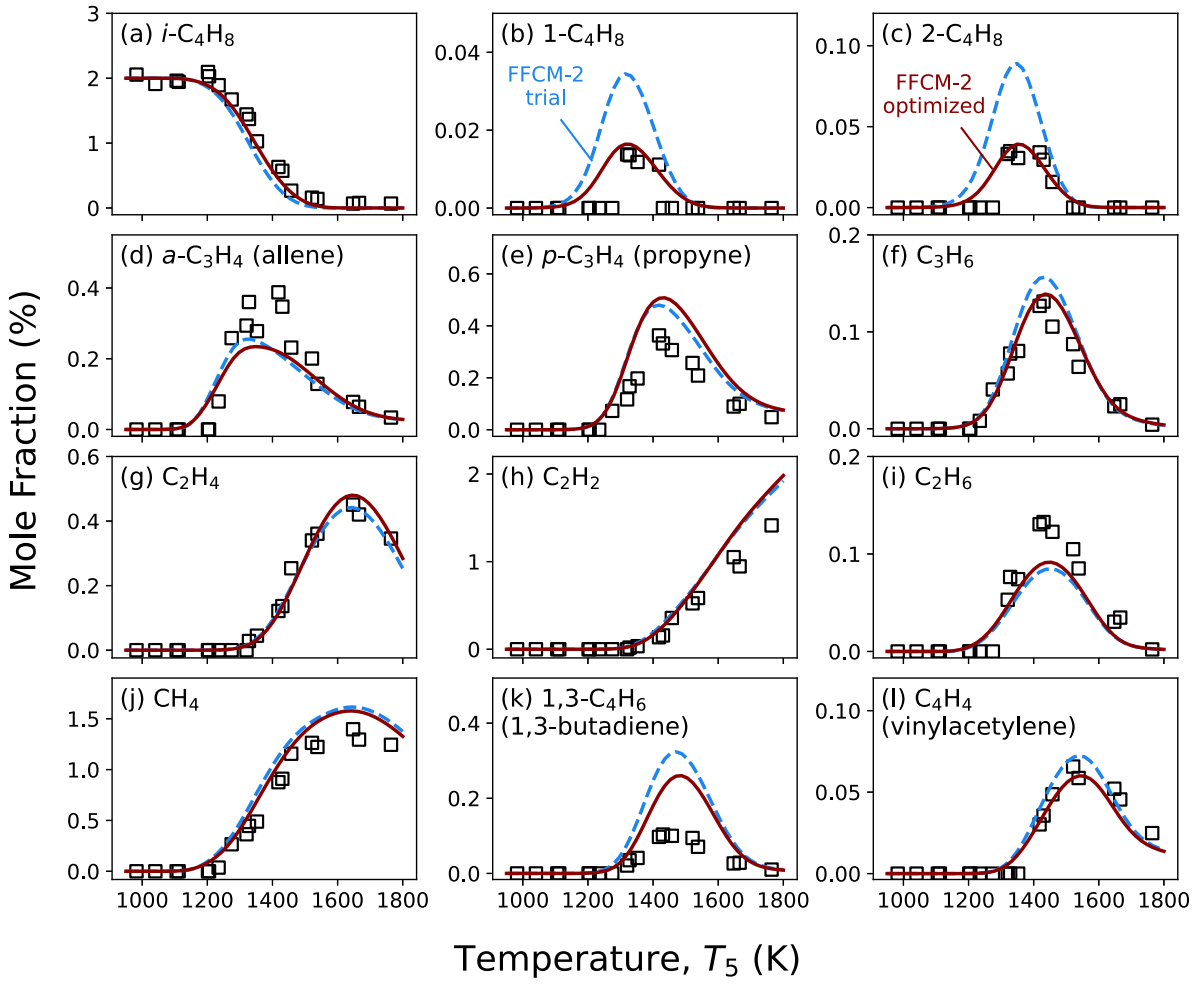

Fig. 2. Pyrolysis of 2% i-C_4H_8 in Ar at $p_5 = 2$ atm, over the temperature range of $T_5 = 982 - 1764$ K. Symbols are experimental data (Nagaraja et al. [30]). The dashed and solid lines represent predictions by the trial and optimized FFCM-2, respectively.

random variable, and the mean $\mathbf{x}^{(0)*}$ is the optimized rate parameter. Using the Bayes' rule, the posterior covariance matrix may be obtained analytically as

$$\mathbf{\Sigma}^* = \mathbf{x}^{(1)*}\mathbf{x}^{(1)*\mathrm{T}} = \Big(\sum_{m=1}^{M} \frac{\mathbf{J}_\mathbf{m}^\mathrm{T}\mathbf{J}_\mathbf{m}}{\sigma_{m,obs}^2} + \lambda^2\mathbf{I}\Big)^{-1}, \tag{12}$$

where $\mathbf{J_m} = (\partial y_m/\partial \mathbf{x})|_{\mathbf{x}=\mathbf{x}^{(0)*}}$ is the Jacobian matrix of the mth target evaluated at the optimal point, and $\mathbf{I}$ is the identity matrix. Clearly, the covariance matrix of the trial model is a diagonal matrix, given as $\lambda^{-2}\mathbf{I}$.

Following the approach of polynomial chaos expansions [23], the model prediction uncertainties can be evaluated analytically using

$$\sigma_m^{*2} = \|\mathbf{J}_\mathbf{m}^\mathrm{T}\mathbf{L}\|_2^2 + \frac{1}{2}\|\mathbf{L}^\mathrm{T}\mathbf{H_m}\mathbf{L}\|_F^2 , \tag{13}$$

where $\mathbf{J_m}$ and $\mathbf{H_m}$ are the Jacobian and Hessian matrices, respectively, and $\mathbf{L}$ is the Cholesky decomposition of the covariance matrix ($\mathbf{\Sigma} = \mathbf{L}\mathbf{L}^\mathrm{T}$). The subscripts 2 and F stand for the Euclidean norm and the Frobenius norm, respectively.

2.3. HyChem model and its parameters

The two aviation fuels considered are the Gevo ATJ fuel (POSF 11498) and a conventional Jet A (POSF10325), where the POSF number refers to the fuel batch number designated by the National Jet Fuels Combustion Program [19]. In the HyChem formulation, the ATJ fuel (POSF11498) is represented as ($C_{13}H_{28}$) [3] and the lumped fuel reactions are

$$C_{13}H_{28} \rightarrow e_{d,1}(i\text{-}C_4H_8 + \omega_3 C_3H_6 + \omega_2 C_2H_4) + \alpha_1 H + (2-\alpha_1)CH_3 , \tag{14}$$

$$C_{13}H_{28} + R \rightarrow RH + e_{a,1}(i\text{-}C_4H_8 + \omega_3 C_3H_6 + \omega_2 C_2H_4) + \beta_1 H + (1-\beta_1)CH_3 . \tag{15}$$

Similarly, we consider $C_{11}H_{22}$ for Jet A (POSF10325) [2]:

$$C_{11}H_{22} \rightarrow e_{d,2}(C_2H_4 + \lambda_3 C_3H_6 + \lambda_{4,i} i\text{-}C_4H_8 + \lambda_{4,1} 1\text{-}C_4H_8) + b_d[\chi C_6H_6 + (1-\chi)C_7H_8] + \alpha_2 H + (2-\alpha_2)CH_3 , \tag{16}$$

$$C_{11}H_{22} + R \rightarrow RH + \gamma CH_4 + e_{a,2}(C_2H_4 + \lambda_3 C_3H_6 + \lambda_{4,i} i\text{-}C_4H_8 + \lambda_{4,1} 1\text{-}C_4H_8) + b_a[\chi C_6H_6 + (1-\chi)C_7H_8] + \beta_2 H + (1-\beta_2)CH_3 . \tag{17}$$

where R = H, CH_3, OH, O_2, HO_2, and O. The HyChem parameters are summarized in Table 1. There are four independent stoichiometric parameters (ω_3, ω_2, α_1, β_1) and seven rate coefficients to be determined for ATJ. For Jet A, we have seven independent stoichiometric coefficients (λ_3, $\lambda_{4,i}$, $\lambda_{4,1}$, γ, χ, α_2, β_2) and seven rate coefficients. The stoichiometric parameters $e_{d,1}$, $e_{a,1}$, $e_{d,2}$, $e_{a,2}$, b_d and b_a are dependent variables due to C and H elemental conservation [2,3].

The HyChem formulation and the underlying assumptions are the same as those in the earlier HyChem work [1–3]. Differing from the

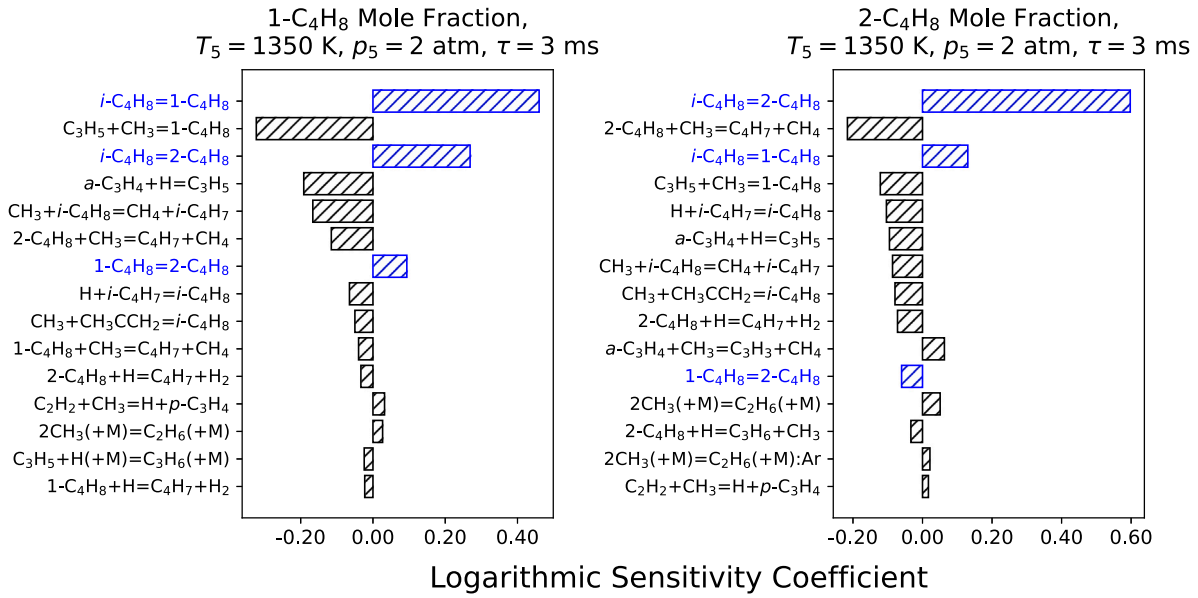

Fig. 3. Ranked sensitivity coefficients computed for 1-C_4H_8 and 2-C_4H_8 yields in shock tube pyrolysis of 2% i-C_4H_8 in Ar at $T_5 = 1352$ K, $p_5 = 2$ atm, and 3 ms residence time.

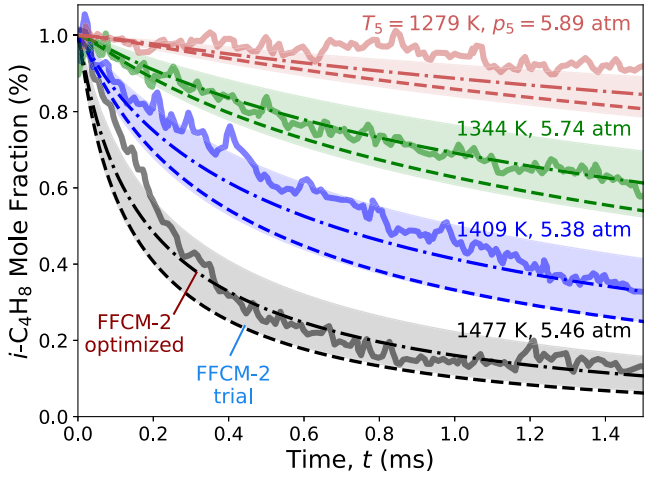

Fig. 4. Shock tube speciation time history predicted by the trial and optimized FFCM-2 for the pyrolysis of 1% i-C_4H_8 in Ar at various temperatures and pressure p_5 near 5.5 atm. The solid lines are experimental data [29]. The dashed-dot-dashed lines represent the optimized FFCM-2, and the dashed lines represent the trial FFCM-2. The shaded areas show the temperature sensitivity (±15 K) calculated using the optimized FFCM-2.

earlier effort is the use of FFCM-2 as an improved foundational fuel chemistry model (rather than USC Mech II). In the current work, we demonstrate and document how HyChem parameters are updated when USC Mech II is replaced by FFCM-2. More importantly, we assess the HyChem model uncertainty by considering the remaining uncertainty of the optimized FFCM-2. To determine the updated HyChem parameters, we consider an inverse problem given by

$$\Phi_2(\mathbf{x}) = \min_{\mathbf{x}} \sum_{m=1}^{M} \left(\frac{y_m(\mathbf{x}) - y_{m,obs}}{\sigma_{m,obs}} \right)^2, \tag{18}$$

where $y_{m,obs}$ and $\sigma_{m,obs}$ refers to the mth speciation target data and its uncertainty, respectively. As in the previous studies [2,3], the global combustion properties (laminar flame speed and ignition delay time) are used for model validation and testing only; they are not used as the targets in HyChem parameter determination, thus differing from FFCM-2 optimization, which considered both species measurements and global combustion properties as optimization targets. For the flow reactor experiments, we consider the species time-histories after 3 ms of the reaction time as discussed in [2,3]. We considered all measured foundational fuels/species as targets (C_2H_4, C_3H_6, i-C_4H_8, 1-C_4H_8, CH_4, C_2H_2, a-C_3H_4, p-C_3H_4, C_6H_6, $C_6H_5CH_3$). For shock tube species, all experiments discussed in [2] were considered as targets. Targets were selected over intervals of every 0.25 ms. The optimized foundational fuel chemistry model, FFCM-2, was frozen during HyChem parameter determination. The reactions and rate constants of $C_{5\text{-}7}$ species of USC Mech II are appended to FFCM-2 to account for the aromatic chemistry. Low- and NTC-enabled HyChem models are also available through this work, and the model formations are discussed in the SM Section S8.

2.4. Kinetic simulations

Simulations used Cantera (version 2.6.0) interfaced with Python [51]. For ignition delay times, we obtained the time histories by solving the initial value problems under the constant-volume condition, using the `IdealGasReactor` module. Ignition delay times are then determined using methods that are consistent with the experiments. Shock tube species were simulated using the `IdealGasConstPressureReactor` module, under constant pressure. Flow reactor species time histories were simulated under the constant-temperature, constant-pressure condition, at starting time around 3 ms with initial conditions, as discussed in [2,3]. For laminar flame speeds, we implemented the `FreeFlame` module. Each flame is computed on at least 400 mesh grids, with thermal diffusion and multi-component transport.

3. Results and discussion

3.1. iso-Butene pyrolysis and oxidation

We first focus on the *iso*-butene (i-C_4H_8) submodel of FFCM-2. Under high-temperature pyrolytic conditions, the consumption of i-C_4H_8

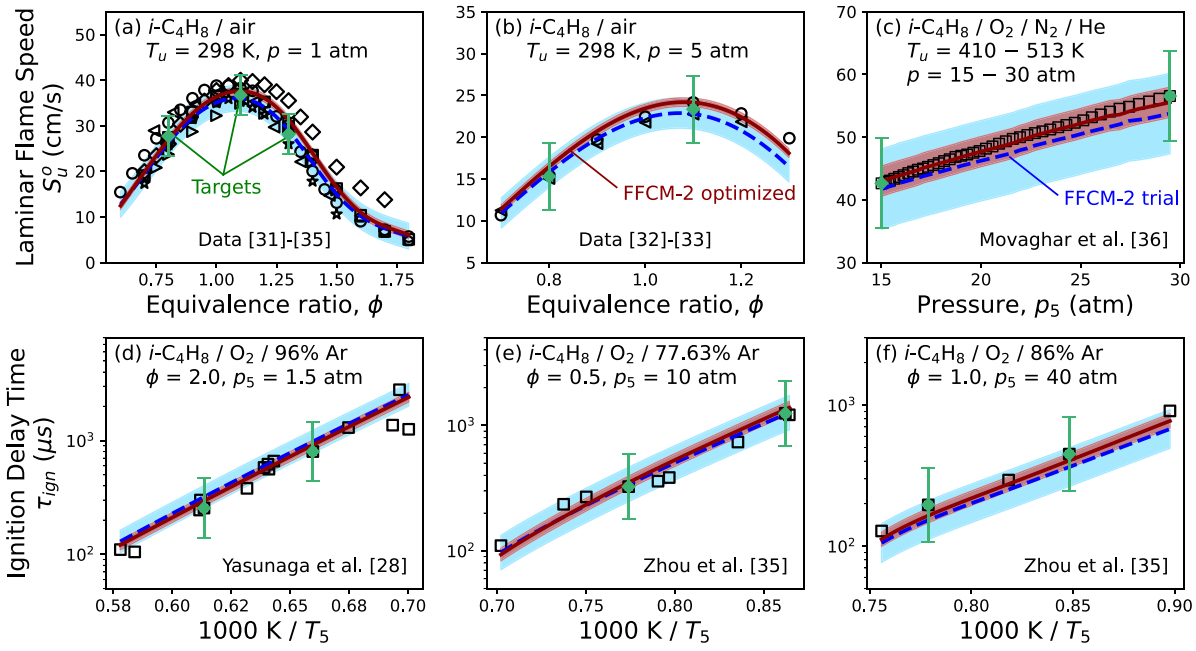

Fig. 5. Laminar flame speed and ignition delay time of several i-C_4H_8 mixtures. Symbols are experimental data. In panel (a), ◇: Davis and Law [31], □: Kelly [32], ○: Zhao et al. [33], ☆: Park et al. [34], ○: Zhou et al. [35] (CNRS data), ◁: Zhou et al. (Princeton data) [35], ▷: Zhou et al. (Texas A&M data) [35]. In panel (b), ◁: Kelly [32], ○: Zhao et al. [33]. The dashed lines and solid lines are model predictions by the trial and optimized FFCM-2. The shaded areas are the 2σ model prediction uncertainty bounds. The filled diamonds with error bars are the experimental targets considered in FFCM-2 optimization and their 2σ uncertainties.

is initiated by the C–H fission of i-C_4H_8 to produce a resonantly-stabilized i-C_4H_7 (2-methylallyl) radical, and to a lesser extent, its isomerization to form 1-C_4H_8 and 2-C_4H_8. i-C_4H_8 also undergoes hydrogen abstraction by H and CH_3 to form i-C_4H_7. The resonantly-stabilized i-C_4H_7 radical is a major intermediate during i-C_4H_8 pyrolysis. It undergoes further decomposition to produce CH_3 and allene (a-C_3H_4). The latter equilibrates quickly with propyne (p-C_3H_4). Chemically activated reactions involving H addition followed by C–C fission to form C_3H_6 and CH_3 can be important also under some conditions. Fig. 2 shows comparisons of the experiment [30] and model predictions for the major and minor species in shock tube pyrolysis of 2% i-C_4H_8 in Ar at $p_5 = 2$ atm, over the temperature range of $T_5 = 982 - 1764$ K. Two observations can be made. First, the trial model yields predictions that are generally in good agreement with the experiment. The model over-predicts the production of 1-C_4H_8 and 2-C_4H_8, as we had expected, because the trial assignments of the rate coefficients for reactions (1) and (2) are rather tentative. Fig. 3 shows the peak yields of 1-C_4H_8 and 2-C_4H_8 to be sensitive to the isomerization from i-C_4H_8. FFCM-2 optimization used the mole fractions of 1-C_4H_8 and 2-C_4H_8 at 1352 K as part of the optimization targets, and reduced the A-factors of reactions (1) and (2) to 44% and 35% of their trial values, respectively. These changes are well within the uncertainty bounds we assigned initially. The yields of 1-C_4H_8 and 2-C_4H_8 predicted with the optimized FFCM-2 are now in close agreement with the experiment (Fig. 2b&c). In Fig. S4, the trial and optimized isomerization reaction rate coefficients are compared with that of the C–H fission reaction (i-$C_4H_8 \rightleftharpoons i$-$C_4H_7$ + H), showing that the optimized isomerization rates are comparable to that of the C–H fission reaction, thus explaining the top sensitivity observed for these initiation reactions during shock tube pyrolysis of *iso*-butene.

Another observation from Fig. 2 is that both trial and optimized FFCM-2 over-predicts propyne (p-C_3H_4) and 1,3-butadiene (1,3-C_4H_6) concentrations and under-predicts allene (a-C_3H_4) and ethane (C_2H_6) concentrations above 1400 K. The discrepancy is explained by missing benzene chemistry in FFCM-2 as the model truncates at C_4. To illustrate this point, the $C_{5\text{-}7}$ aromatics chemistry (benzene and toluene) of USC Mech II was appended to the optimized FFCM-2; and the resulting model is improved for these species (Fig. S2 of the SM).

Time histories of i-C_4H_8 as measured during its pyrolysis in the Stanford shock tube [29] are also considered as targets. Fig. 4 compares the model predictions against experimental data, where the shaded areas represent $T_5 \pm 15$ K temperature sensitivity calculated by the optimized FFCM-2. As shown, the trial model (dashed lines) over-predicts the i-C_4H_8 consumption rates, while the optimized model predicts the rates well within the expected data uncertainty. The optimization indicates that key rate coefficients impacting i-C_4H_8 pyrolysis include reactions (2), (3), and (6) (Section S4 of the SM). The rate coefficients of the two isomerization reactions (reactions (2) and (3)) were changed significantly from the trial assignments, with the optimized-to-trial rate ratios of 0.34 and 0.45, respectively. These changes are not surprising considering that the initial assignments using reaction rate theories were rather tentative and approximate. Changes to other i-C_4H_8 reactions are smaller, and within 30% of the original estimates. In Fig. S3, we compared the mean and 95% confidence interval of some key i-C_4H_8 reaction rate coefficients before and after uncertainty minimization, showing that all changes are within the uncertainty bounds initially assigned to the rate parameters.

The optimized FFCM-2 is validated and tested against the global combustion properties (laminar flame speeds and ignition delay times) over a wide range of thermodynamic conditions. Fig. 5 shows selected results of the trial and optimized FFCM-2 on i-C_4H_8 flame speed and ignition delay. In each panel, the experimental targets considered in FFCM-2 optimization are marked by the filled symbols with error bars. It can be seen that in comparison with the trial model, the optimized FFCM-2 improves the prediction accuracy. As importantly, the prediction uncertainties of the optimized model are significantly reduced from the trial model, as evidenced by the narrowed 2σ bands plotted. Notably, the optimized model gives significantly reduced prediction uncertainty in the laminar flame speed and ignition delay at elevated pressures (Fig. 5c&f).

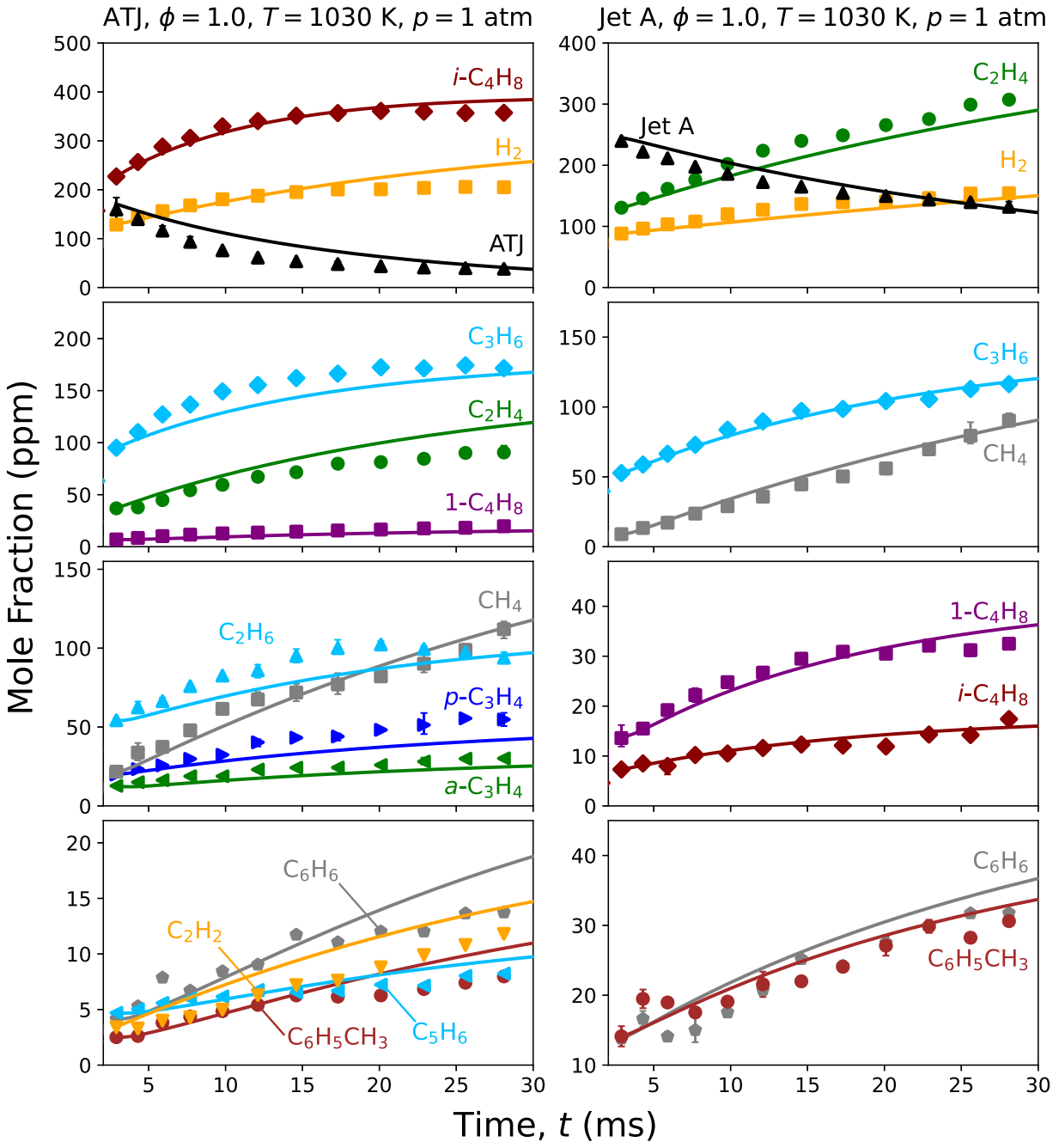

Fig. 6. Time histories of key species during the oxidation of ATJ (left column, 305 ppm ATJ in a vitiated O_2-N_2 mixture at $\phi = 1$) and Jet A (right column, 314 ppm Jet A in a vitiated O_2-N_2 mixture at $\phi = 1$) in the Stanford flow reactor at temperature $T = 1030$ K and pressure $p = 1$ atm. Symbols are experimental data: ATJ [3] and Jet A [2]. Lines are calculations using the respective HyChem ATJ and Jet A models. Simulation starts at 2.87 ms using measured species concentrations as the input (see, [2,3]).

3.2. ATJ and Jet A models

Using FFCM-2 as the foundational fuel chemistry model (with addition of the USC Mech II benzene and toluene chemistry), we re-examined the earlier HyChem models for ATJ [3] and Jet A [2] combustion. As discussed before, the HyChem parameters were determined through a subsequent inverse problem using pyrolysis and oxidative pyrolysis speciation data [2,3]. The resulting parameter values are provided in Table S1 (Section S5 of the SM). Fig. 6 presents the experimental data and model results for oxidative pyrolysis of ATJ and Jet A (310 PPM fuel in vitiated O_2-N_2 mixtures at 1.0 equivalence ratio, 1030 K temperature and 1 atm pressure). As seen, the HyChem models capture the time histories of the major and minor species well. Fig. 7 presents similar comparisons for shock tube pyrolysis of ATJ focusing on four key pyrolysis products: i-C_4H_8, C_3H_6, C_2H_4 and CH_4. Likewise, the Jet A model reproduces also key species data: C_2H_4 and CH_4. Furthermore, Fig. S5 shows the HyChem model captures the measured C_2H_4 yields in both pyrolysis and oxidative pyrolysis of Jet A at several reaction times.

3.3. ATJ and Jet A HyChem model validation against global combustion properties

A key aspect of the HyChem model development is that it relies on the shock tube and flow reactor speciation data for model parameter determination. Global combustion properties (e.g., laminar flame speed

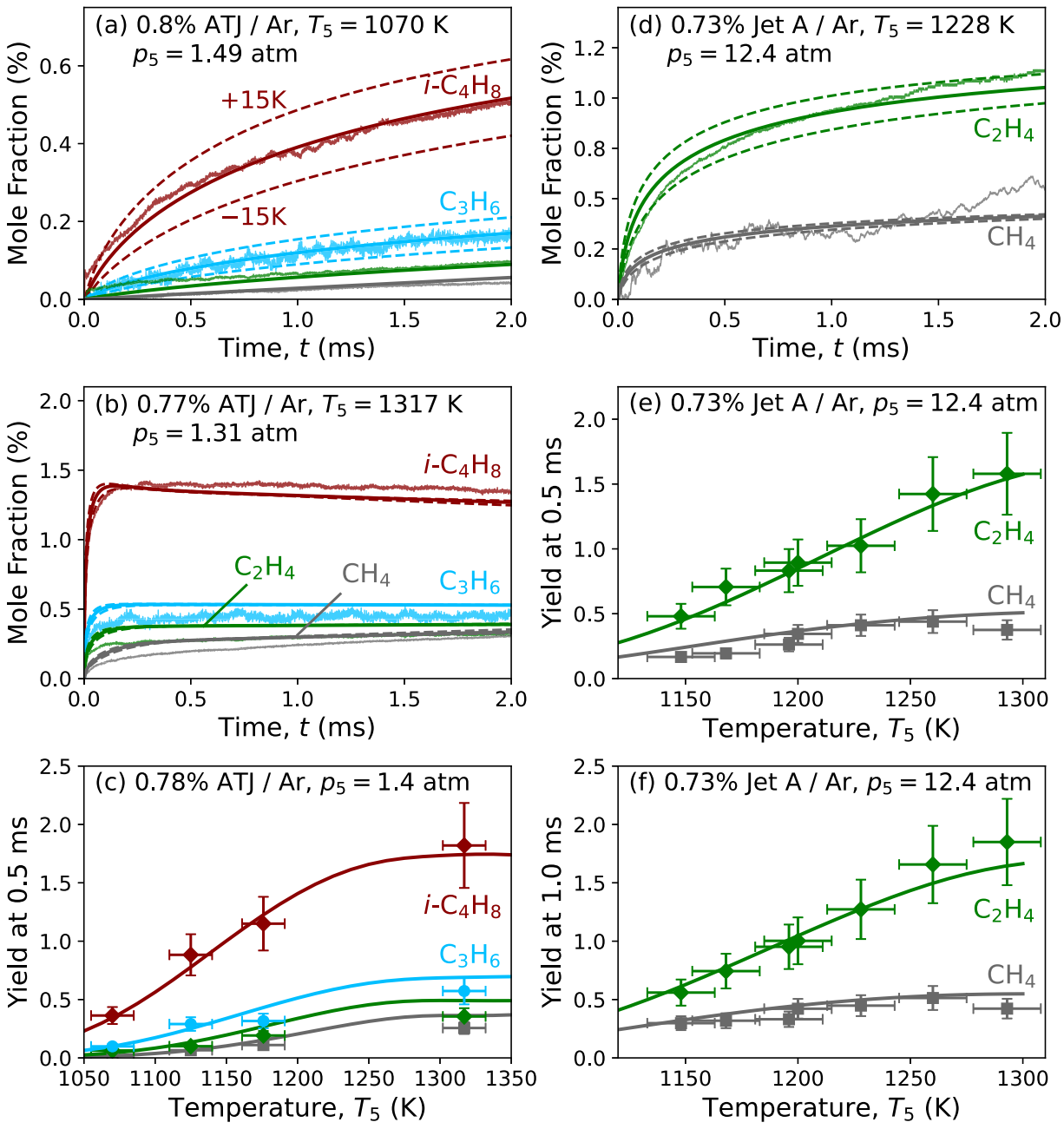

Fig. 7. Selected shock tube speciation data (symbols and lines with data noises) for ATJ [3] and Jet A [2] pyrolysis and current HyChem model simulations (solid lines). (a) 0.8% ATJ in Ar at $T_5 = 1070$ K and $p_5 = 1.49$ atm, (b) 0.77% ATJ in Ar at $T_5 = 1317$ K and $p_5 = 1.31$ atm, (c) 0.77% ATJ in Ar at $p_5 = 1.4$ atm and residence time $\tau = 0.5$ ms, (d) 0.73% Jet A in Ar at $T_5 = 1228$ K and $p_5 = 12.4$ atm, (e) 0.73% Jet A in Ar at $p_5 = 12.4$ atm and $\tau = 0.5$ ms, and (f) 0.73% Jet A in Ar at $p_5 = 12.4$ atm and $\tau = 1.0$ ms. Dashed lines represent the computed ±15 K temperature sensitivity on the species mole fractions. Vertical error bars in (c), (e) and (f) represent the species measurement uncertainty; horizontal error bars represent ±15 K T_5 uncertainty.

and ignition delay time), are then used to test a model. As shown in Fig. 8, the current HyChem model reproduce well the laminar flame speed and ignition delay data of ATJ/air mixtures. Here we considered the flame speed data of Wang et al. [3], and the more recent data of Richter et al. [50], which were collected using a burner flame cone-angle approach. As it can be seen in Fig. 8, the model predicts the fuel-lean flame speed well for all three sets of flame speed data shown. In the fuel rich region, some inconsistency is seen between the two data sources: the HyChem model predicts a somewhat higher flame speed value than the data of [3], while it produces a lower value than the data of Richter et al. [50]. Overall, the model predictions are well within the 2σ uncertainties of the respective measurements for both the flame speed and shock tube ignition delay. Plots for Jet A are shown in Fig. 9 with similar observations: the updated HyChem model reproduce the laminar flame speed and shock tube ignition delay data available from [2] within the measurement uncertainties.

Critical to the current effort is an assessment of the impact of FFCM-2 uncertainty minimization on the HyChem models. We show in Figs. 8 and 9 the HyChem prediction uncertainties for each of the global combustion properties considered. As the foundation model, the optimized and uncertainty minimized FFCM-2 produces significantly improved HyChem model prediction accuracy than using unoptimized, trial FFCM-2. Critically, the uncertainty band sizes are reduced

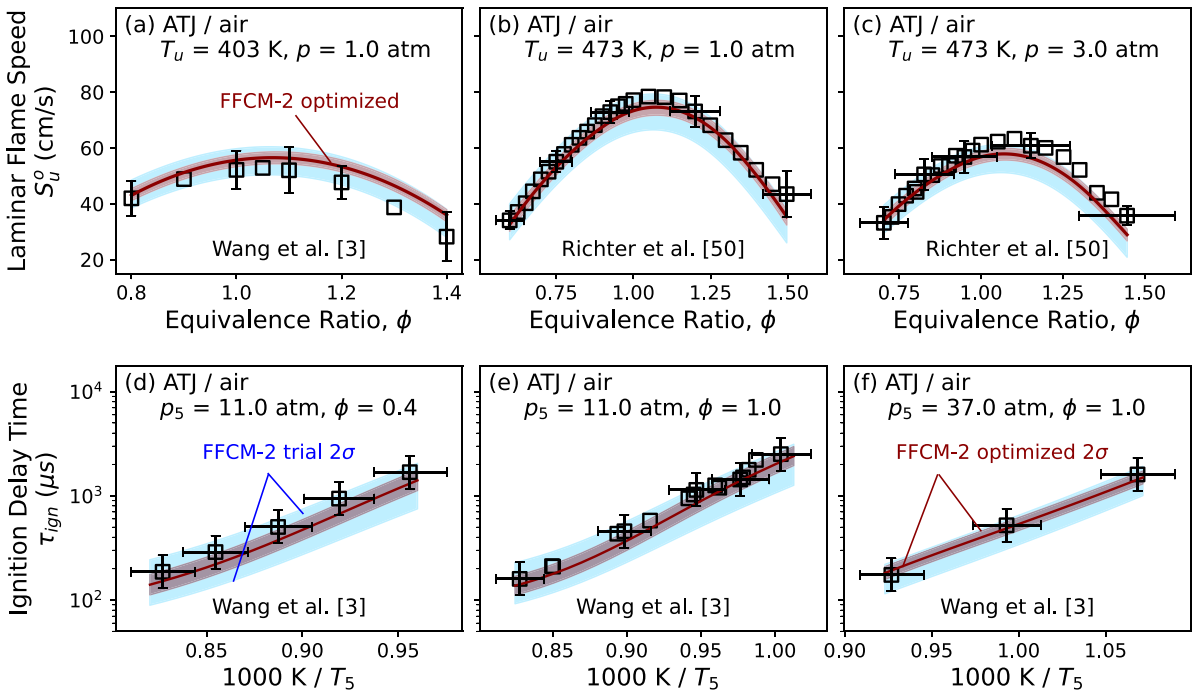

Fig. 8. Experimental (symbols, Wang et al. [3] and Richter et al. [50]) laminar flame speed and ignition delay time of ATJ/air mixtures compared to predictions (lines) of the updated HyChem model. The shaded areas show prediction uncertainties (95% confidence intervals), comparing optimized and uncertainty minimized FFCM-2 with its trial version of the model. Error bars represent 2σ data uncertainty.

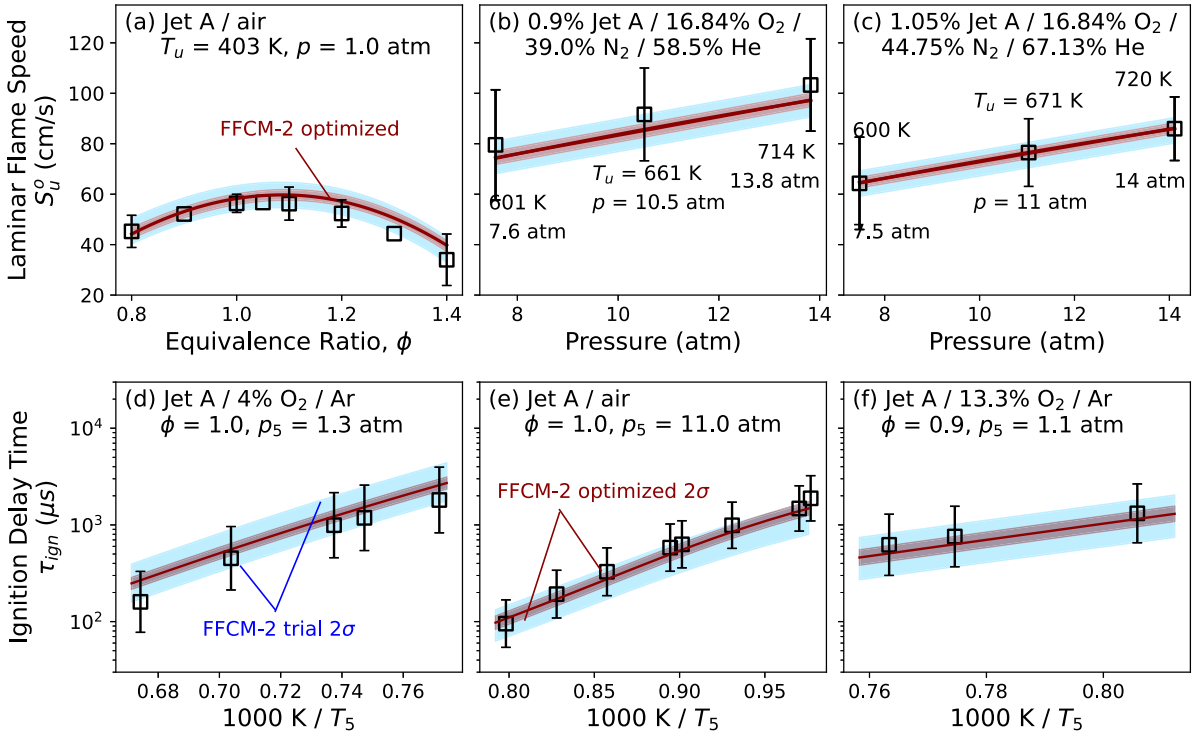

Fig. 9. Experimental (symbols [2]) laminar flame speed of and ignition delay time of Jet A/O_2/diluent mixtures compared to predictions (lines) of the updated HyChem model. The shaded areas show prediction uncertainties (95% confidence intervals), comparing optimized and uncertainty minimized FFCM-2 with its trial version of the model. Error bars are 2σ uncertainty of selected data points.

significantly when the optimized FFCM-2 compared to the trial FFCM-2. The impact is particularly large at elevated pressures than at the ambient pressure. The results shown illustrates again that our ability to predict the combustion properties of large, real liquid fuels lies largely in the accuracy of the foundational fuel chemistry model, as discussed in [2,3,18].

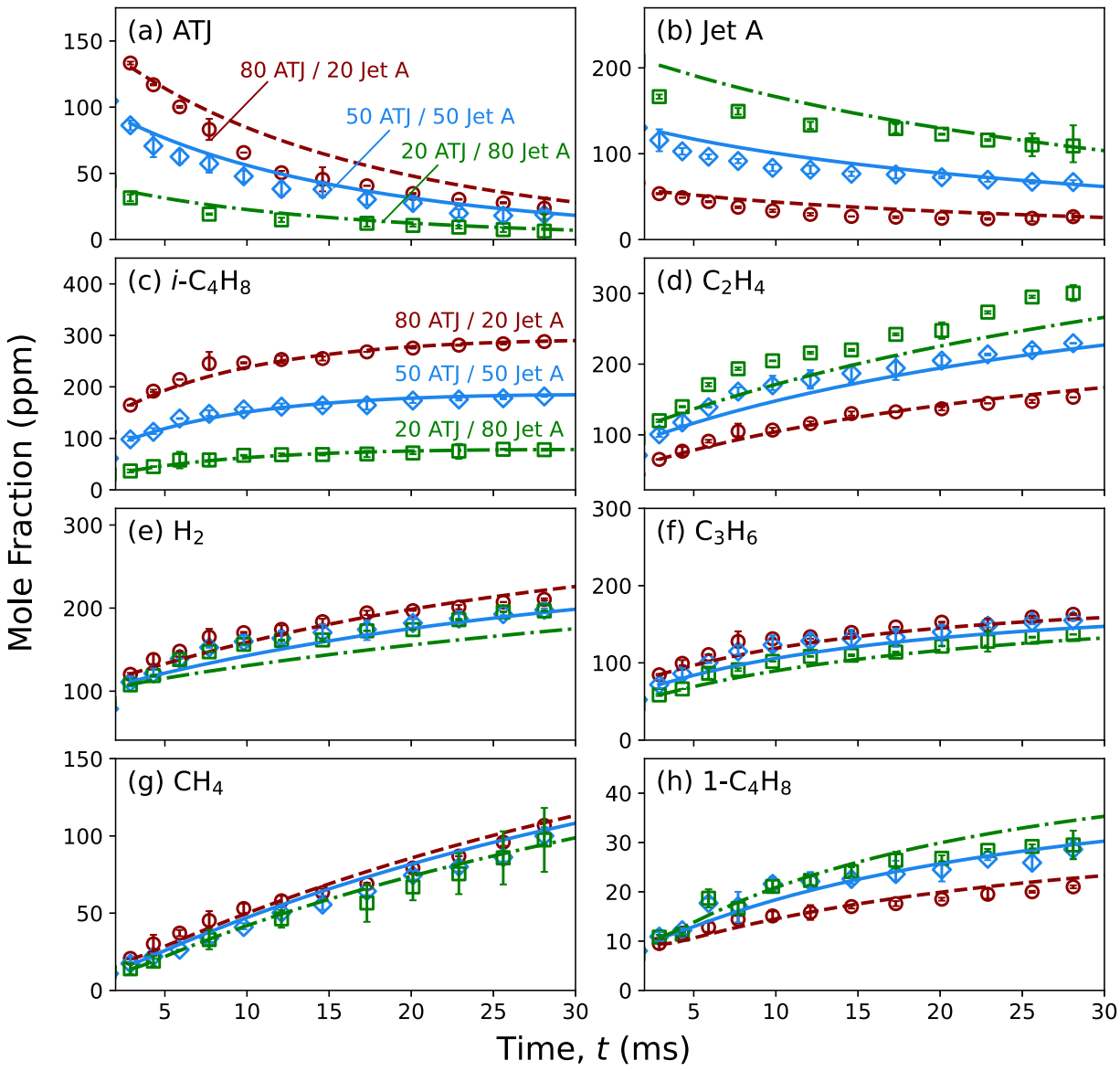

Fig. 10. Experimental (symbols [3]) and computed (lines) species time history during oxidative pyrolysis of several 310 ppm ATJ/Jet A fuel blends in the Stanford flow reactor at temperature $T_5 = 1030$ K, pressure $p_5 = 1$ atm and equivalence ratio $\phi = 1.0$.

3.4. ATJ-Jet A blends

Owing to the relatively shorter time scale of fuel decomposition than fragment oxidation, the pyrolytic reaction kinetics of blends of two real fuels typically do not couple with each other, and as such the HyChem models developed for each fuel can be simply added to each other to make appropriate predictions for the blends [3]. Such an "additive" behavior is consistent with the fast time scales for the thermal decomposition of both fuels during their combustion. To again illustrate this point, we plot in Fig. 10 key species time histories of three ATJ-Jet A blends (20%/80%, 50%/50% and 80%/20%) during the early stage of their stoichiometric oxidation in the Stanford flow reactor ($T = 1030$ K, $p = 1$ atm) [3]. Consistently, both the experiment and model show the "additive" behavior in the decomposition species. Figure S6 of the SM presents a similar comparison for a fuel-rich case ($\phi = 2$). Figure S7 of the SM further shows that the simple "additive" HyChem model reproduces the shock tube yield of C_2H_4, C_3H_6 and i-C_4H_8 for the same three ATJ/Jet A blends. In all cases, the production of C_3H_6 is invariant with respect to fuel blending as one would expect.

Fig. 11 shows that the combined ATJ-Jet A HyChem models captures the effect of blending on the ignition delay at two blending ratios: 50% ATJ – 50% Jet A and 20% ATJ – 80% Jet A. The impact of FFCM-2 uncertainty minimization is again illustrated here. While the HyChem blended model using trial FFCM-2 reproduces the ignition delay data closely, the prediction uncertainty remains large, by as much as ±50%, for the ignition delay time considered. With the uncertainty-minimized FFCM-2, the HyChem prediction uncertainty is reduced significantly, to about ±15%–20%, as shown by the 2σ bands of the predictions in Fig. 11.

The critical impact of the foundational fuel chemistry model on the prediction of combustion properties of real fuels may be understood by examining Fig. S8 of the SM, where sensitivity spectra are shown for the mixtures of Fig. 11, all at $T_5 = 1400$ K. HyChem-specific rate parameters play little role in the ignition delay predictions. For all cases $H + O_2 \rightleftharpoons O + OH$ is the dominating reaction that impacts the ignition delay. Further, we observed that the ignition delay of neat ATJ is sensitive to the i-C_4H_8 chemistry (Fig. S8a). Notably, i-$C_4H_8 + H \rightleftharpoons i$-$C_4H_7 + H_2$ and i-$C_4H_8 + H \rightleftharpoons C_3H_6 + CH_3$ are both ranked among

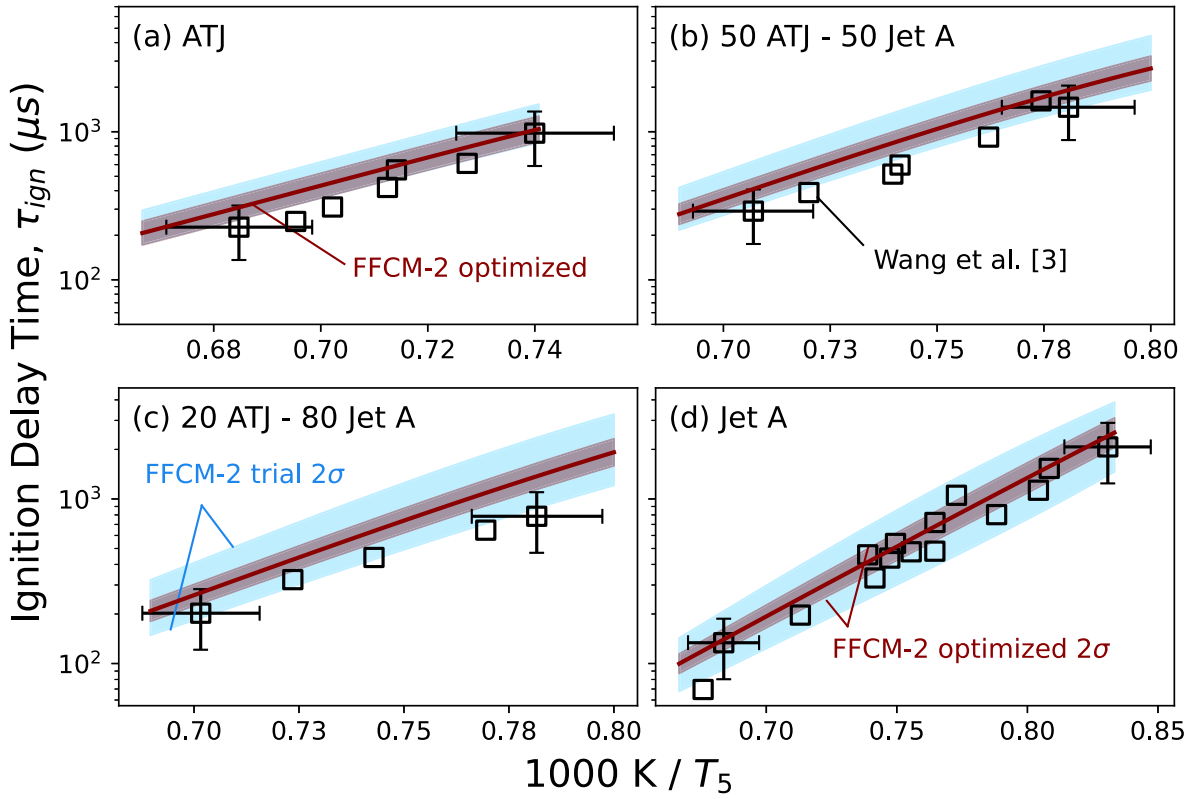

Fig. 11. Experimental (symbols, [3]) and computed (lines) ignition delay time of stoichiometric ATJ and Jet A in air and two stoichiometric ATJ/Jet A blends in air, at $p_5 = 0.56$ atm. Error bars are data uncertainties [3]. Shaded areas are prediction uncertainties of the trial and optimized FFCM-2.

the top reactions. The H-abstraction of i-C_4H_8 by OH is also found in the list. In comparison, the ignition delay of Jet A is sensitive to a different set of reactions. Apart from $H + O_2 \rightleftharpoons O + OH$, the reactions involving C_3H_6 and the allyl radical (a-C_3H_5) impact the oxidation rate. The H-abstraction of C_2H_4 by OH also promoted the reactivity. For the fuel blends, we again observe very little sensitivities from the fuel-specific reactions or the HyChem parameters on the ignition delay time. Because the sensitivity is overwhelmingly skewed toward the foundational fuel chemistry, the tightening of the FFCM-2 uncertainty also leads to the tightening of the HyChem prediction uncertainty. In fact, the HyChem model uncertainties are smaller than the uncertainty of the corresponding real-fuel experiments, as it can be seen in Fig. 11 as well as Figs. 8 and 9.

NTC-enabled HyChem models are also available from the current study for the ATJ and Jet A fuels. The development of these models are discussed in Section S9 of the SM. The model formulations follow that of [2], and the comparisons to the experimental ignition delay times covering high-, NTC- and low-temperature regions are provided in Figs. S9, S10, and S11 of the SM. Lastly, we note that both the high-temperature and NTC-enabled HyChem models are available in Chemkin and Cantera formats from https://web.stanford.edu/group/haiwanglab/FFCM2/docs/Application/.

4. Conclusions

In the current study, we updated the HyChem combustion reaction models for Gevo ATJ and a typical Jet A using the recently developed Foundational Fuel Chemistry Model version 2 (FFCM-2). A part of our focus was on the *iso*-butene submodel of FFCM-2, showing that the optimized and uncertainty-minimized FFCM-2 model is capable of reproducing a large body of *iso*-butene pyrolysis and oxidation data with significantly reduced prediction uncertainties. Further to this effort, we demonstrate that uncertainty minimization of FFCM-2 is crucial to making accurate predictions of the combustion properties of real, multi-component liquid fuels through the HyChem approach. A systematic framework is also established for determining HyChem submodel parameters, using as targets the thermal and oxidative pyrolysis data measured in shock tube or flow reactor. The updated HyChem models are shown to accurately predict the global combustion properties for ATJ and Jet A. Of equal importance, the prediction uncertainties show appreciable reduction owing to the minimized uncertainties in FFCM-2. The two HyChem models can simply be combined to make useful predictions for the combustion properties of ATJ/Jet A blends.

CRediT authorship contribution statement

Yue Zhang: Performed research, Writing – original draft. **Wendi Dong:** Performed research. **Rui Xu:** Performed research, Writing – original draft. **Gregory P. Smith:** Performed research, Conceived and designed research, Writing – original draft. **Hai Wang:** Conceived and designed research, Writing – original draft.

Declaration of competing interest

The authors declare that they have no known competing financial interests or personal relationships that could have appeared to influence the work reported in this paper.

Acknowledgments

We acknowledge support through the Office of Naval Research (ONR), United States Grant No. N00014-22-1-2606 with Dr. Steve Martens as Program Manager and Grant No. N00014-21-1-2475 with Dr. Eric Marineau as Program Manager.

Appendix A. Supplementary data

Supplementary material related to this article can be found online at https://doi.org/10.1016/j.combustflame.2023.113168.

References

[1] H. Wang, R. Xu, K. Wang, C.T. Bowman, R.K. Hanson, D.F. Davidson, K. Brezinsky, F.N. Egolfopoulos, A physics-based approach to modeling real-fuel combustion chemistry - I. Evidence from experiments, and thermodynamic, chemical kinetic and statistical considerations, Combust. Flame 193 (2018) 502–519.

[2] R. Xu, K. Wang, S. Banerjee, J. Shao, T. Parise, Y. Zhu, S. Wang, A. Movaghar, D.J. Lee, R. Zhao, X. Han, Y. Gao, T. Lu, K. Brezinsky, F.N. Egolfopoulos, D.F. Davidson, R.K. Hanson, C.T. Bowman, H. Wang, A physics-based approach to modeling real-fuel combustion chemistry – II. Reaction kinetic models of jet and rocket fuels, Combust. Flame 193 (2018) 520–537.

[3] K. Wang, R. Xu, T. Parise, J. Shao, A. Movaghar, D.J. Lee, J.-W. Park, Y. Gao, T. Lu, F.N. Egolfopoulos, D.F. Davidson, R.K. Hanson, C.T. Bowman, H. Wang, A physics-based approach to modeling real-fuel combustion chemistry – IV. HyChem modeling of combustion kinetics of a bio-derived jet fuel and its blends with a conventional Jet A, Combust. Flame 198 (2018) 477–489.

[4] Y. Tao, R. Xu, K. Wang, J. Shao, S.E. Johnson, A. Movaghar, X. Han, J.-W. Park, T. Lu, K. Brezinsky, F.N. Egolfopoulos, D.F. Davidson, R.K. Hanson, C.T. Bowman, H. Wang, A Physics-based approach to modeling real-fuel combustion chemistry – III. Reaction kinetic model of JP10, Combust. Flame 198 (2018) 466–476.

[5] R. Xu, C. Saggese, R. Lawson, A. Movaghar, T. Parise, J. Shao, R. Choudhary, J.-W. Park, T. Lu, R.K. Hanson, D.F. Davidson, F.N. Egolfopoulos, A. Aradi, A. Prakash, V.R.R. Mohan, R. Cracknell, H. Wang, A physics-based approach to modeling real-fuel combustion chemistry – VI. Predictive kinetic models of gasoline fuels, Combust. Flame 220 (2020) 475–487.

[6] C. Saggese, K. Wan, R. Xu, Y. Tao, C.T. Bowman, J.-W. Park, T. Lu, H. Wang, A physics-based approach to modeling real-fuel combustion chemistry – V. NO_x formation from a typical Jet A, Combust. Flame 212 (2020) 270–278.

[7] L. Esclapez, P.C. Ma, E. Mayhew, R. Xu, S. Stouffer, T. Lee, H. Wang, M. Ihme, Fuel effects on lean blow-out in a realistic gas turbine combustor, Combust. Flame 181 (2017) 82–99.

[8] A. Felden, L. Esclapez, E. Riber, B. Cuenot, H. Wang, Including real fuel chemistry in LES of turbulent spray combustion, Combust. Flame 193 (2018) 397–416.

[9] X. Zhao, Y. Tao, T. Lu, H. Wang, Sensitivities of direct numerical simulations to chemical kinetic uncertainties: spherical flame kernel evolution of a real jet fuel, Combust. Flame 209 (2019) 117–132.

[10] M. Hassanaly, Y. Tang, S. Barwey, V. Raman, Data-driven analysis of relight variability of jet fuels induced by turbulence, Combust. Flame 225 (2021) 453–467.

[11] Y. Tang, M. Hassanaly, V. Raman, B.A. Sforzo, J. Seitzman, Probabilistic modeling of forced ignition of alternative jet fuels, Proc. Combust. Inst. 38 (2021) 2589–2596.

[12] L. Gallen, E. Riber, B. Cuenot, Investigation of soot formation in turbulent spray flame burning real fuel, Combust. Flame (2023) 112621.

[13] M. Karalus, P. Thakre, G. Goldin, D. Brandt, Flamelet versus detailed chemistry large eddy simulation for a liquid-fueled gas turbine combustor: a comparison of accuracy and computational cost, J. Eng. Gas Turbines Power 144 (2022) 011004.

[14] A. Panchal, S. Menon, Large eddy simulation of fuel sensitivity in a realistic spray combustor I. Near blowout analysis, Combust. Flame 240 (2022) 112162.

[15] A. Panchal, S. Menon, Large eddy simulation of fuel sensitivity in a realistic spray combustor II. Lean blowout analysis, Combust. Flame 240 (2022) 112161.

[16] Y. Choi, J.F. Driscoll, Scramjet engine flowpath that improves specific impulse using JP-7 fuel, J. Propul. Power 39 (2023) 589–601.

[17] H. Wang, X. You, A.V. Joshi, S.G. Davis, A. Laskin, F. Egolfopoulos, C.K. Law, USC Mech Version II. High-temperature combustion reaction model of H_2/CO/C_1–C_4 compounds, 2007, URL https://ignis.usc.edu:80/Mechanisms/USC-Mech%20II/USC_Mech%20II.htm.

[18] R. Xu, H. Wang, A physics-based approach to modeling real-fuel combustion chemistry – VII. Relationship between speciation measurement and reaction model accuracy, Combust. Flame 224 (2021) 126–135.

[19] M. Colket, J. Heyne, M. Rumizen, M. Gupta, T. Edwards, W.M. Roquemore, G. Andac, R. Boehm, J. Lovett, R. Williams, J. Condevaux, D. Turner, N. Rizk, J. Tishkoff, C. Li, J. Moder, D. Friend, V. Sankaran, Overview of the national jet fuels combustion program, AIAA J. 55 (2017) 1087–1104.

[20] Y. Tao, G. Smith, H. Wang, Critical kinetic uncertainties in modeling hydrogen/carbon monoxide, methane, methanol, formaldehyde, and ethylene combustion, Combust. Flame 195 (2018) 18–29.

[21] G. Smith, Y. Tao, H. Wang, Foundational Fuel Chemistry Model Version 1.0 (FFCM-1), 2016, URL https://web.stanford.edu/group/haiwanglab/FFCM1/.

[22] Y. Zhang, W. Dong, L. Vandewalle, R. Xu, G. Smith, H. Wang, Foundational Fuel Chemistry Model Version 2.0 (FFCM-2), 2023, URL https://web.stanford.edu/group/haiwanglab/FFCM2/.

[23] D.A. Sheen, H. Wang, The method of uncertainty quantification and minimization using polynomial chaos expansions, Combust. Flame 158 (2011) 2358–2374.

[24] H. Wang, D.A. Sheen, Combustion kinetic model uncertainty quantification, propagation and minimization, Prog. Energy Combust. Sci. 47 (2015) 1–31.

[25] Y. Zhang, W. Dong, L.A. Vandewalle, R. Xu, G.P. Smith, H. Wang, Neural network approach to response surface development for reaction model optimization and uncertainty minimization, Combust. Flame 251 (2023) 112679.

[26] H.J. Curran, M.P. Dunphy, J.M. Simmie, C.K. Westbrook, W.J. Pitz, Shock tube ignition of ethanol, isobutene and MTBE: Experiments and modeling, Symp. (Int.) Combust. 24 (1992) 769–776.

[27] J.C. Bauge, F. Battin-Leclerc, F. Baronnet, Experimental and modeling study of the oxidation of isobutene, Int. J. Chem. Kinet. 30 (1998) 629–640.

[28] K. Yasunaga, Y. Kuraguchi, R. Ikeuchi, H. Masaoka, O. Takahashi, T. Koike, Y. Hidaka, Shock tube and modeling study of isobutene pyrolysis and oxidation, Proc. Combust. Inst. 32 (2009) 453–460.

[29] R.M. Spearrin, S. Li, D.F. Davidson, J.B. Jeffries, R.K. Hanson, High-temperature *iso*-butene absorption diagnostic for shock tube kinetics using a pulsed quantum cascade laser near 11.3 μm, Proc. Combust. Inst. 35 (2015) 3645–3651.

[30] S.S. Nagaraja, G. Kukkadapu, S. Panigrahy, J. Liang, H. Lu, W.J. Pitz, H.J. Curran, A pyrolysis study of allylic hydrocarbon fuels, Int. J. Chem. Kinet. 52 (2020) 964–978.

[31] S.G. Davis, C.K. Law, Determination of and fuel structure effects on laminar flame speeds of C_1 to C_8 hydrocarbons, Combust. Sci. Technol. 140 (1998) 427–449.

[32] A.P. Kelley, Dynamics of Expanding Flames (Ph.D. thesis), Princeton University, 2011.

[33] P. Zhao, W. Yuan, H. Sun, Y. Li, A.P. Kelley, X. Zheng, C.K. Law, Laminar flame speeds, counterflow ignition, and kinetic modeling of the butene isomers, Proc. Combust. Inst. 35 (2015) 309–316.

[34] O. Park, P.S. Veloo, D.A. Sheen, Y. Tao, F.N. Egolfopoulos, H. Wang, Chemical kinetic model uncertainty minimization through laminar flame speed measurements, Combust. Flame 172 (2016) 136–152.

[35] C.-W. Zhou, Y. Li, E. O'Connor, K.P. Somers, S. Thion, C. Keesee, O. Mathieu, E.L. Petersen, T.A. DeVerter, M.A. Oehlschlaeger, G. Kukkadapu, C.-J. Sung, M. Alrefae, F. Khaled, A. Farooq, P. Dirrenberger, P.-A. Glaude, F. Battin-Leclerc, J. Santner, Y. Ju, T. Held, F.M. Haas, F.L. Dryer, H.J. Curran, A comprehensive experimental and modeling study of isobutene oxidation, Combust. Flame 167 (2016) 353–379.

[36] A. Movaghar, R. Lawson, F.N. Egolfopoulos, Confined spherically expanding flame method for measuring laminar flame speeds: Revisiting the assumptions and application to C_1–C_4 hydrocarbon flames, Combust. Flame 212 (2020) 79–92.

[37] N. Lokachari, S. Panigrahy, G. Kukkadapu, G. Kim, S.S. Vasu, W.J. Pitz, H.J. Curran, The influence of iso-butene kinetics on the reactivity of di-isobutylene and iso-octane, Combust. Flame 222 (2020) 186–195.

[38] B.L. Kalra, J.Y. Cho, D.K. Lewis, Kinetics of the thermal isomerization of methylcyclopropane, J. Phys. Chem. A 103 (1999) 362–364.

[39] F. Dubnikova, A. Lifshitz, Structural and geometrical isomerizations of cyclopropane. quantum chemical and RRKM calculations, J. Phys. Chem. A 102 (1998) 3299–3306.

[40] J.A. Miller, S.J. Klippenstein, Master equation methods in gas phase chemical kinetics, J. Phys. Chem. A 110 (2006) 10528–10544.

[41] J.R. Barker, Multiple-Well, multiple-path unimolecular reaction systems. I. MultiWell computer program suite, Int. J. Chem. Kinet. 33 (2001) 232–245.

[42] O.K. Rice, H.C. Ramsperger, Theories of unimolecular gas reactions at low pressures, J. Am. Chem. Soc. 49 (1927) 1617–1629.

[43] L.S. Kassel, Studies in homogeneous gas reactions. I, J. Phys. Chem. 32 (2002) 225–242.

[44] R.A. Marcus, Unimolecular dissociations and free radical recombination reactions, J. Chem. Phys. 20 (1952) 359–364.

[45] J. Power, K.P. Somers, S.S. Nagaraja, H.J. Curran, Hierarchical study of the reactions of hydrogen atoms with alkenes: A theoretical study of the reactions of hydrogen atoms with C_2–C_4 alkenes, J. Phys. Chem. A 125 (2021) 5124–5145.

[46] K. Wang, S.M. Villano, A.M. Dean, Fundamentally-based kinetic model for propene pyrolysis, Combust. Flame 162 (2015) 4456–4470.

[47] J.A. Montgomery Jr., M.J. Frisch, J.W. Ochterski, G.A. Petersson, A complete basis set model chemistry. VII. Use of the minimum population localization method, J. Chem. Phys. 112 (2000) 6532–6542.

[48] F. Khaled, J. Badra, A. Farooq, A shock tube study of C_4–C_6 straight chain alkenes + OH reactions, Proc. Combust. Inst. 36 (2017) 289–298.

[49] S.S. Vasu, Z. Hong, D.F. Davidson, R.K. Hanson, D.M. Golden, Shock tube/laser absorption measurements of the reaction rates of OH with ethylene and propene, J. Phys. Chem. A 114 (2010) 11529–11537.

[50] S. Richter, G. Kukkadapu, C.K. Westbrook, M. Braun-Unkhoff, C. Naumann, M. Köhler, U. Riedel, A combined experimental and modeling study of combustion properties of an isoparaffinic alcohol-to-jet fuel, Combust. Flame 240 (2022) 111994.

[51] D.G. Goodwin, H.K. Moffat, I. Schoegl, R.L. Speth, B.W. Weber, Cantera: An object-oriented software toolkit for chemical kinetics, thermodynamics, and transport processes, 2022, Version 2.6.0. https://www.cantera.org.